Cosmic star formation history revealed by the AKARI

& Spatially-resolved spectroscopy of an E+A (Post-starburst) system

Tomotsugu GOTO[*], the AKARI NEPD team[†], M. Yagi[**] and C. Yamauchi[†]

[*]*Institute for Astronomy, University of Hawaii, 2680 Woodlawn Drive, Honolulu, HI, 96822, USA*
[†]*Japan Aerospace Exploration Agency, Sagamihara, Kanagawa 229-8510, Japan*
[**]*National Astronomical Observatory, 2-21-1 Osawa, Mitaka, Tokyo, 181-8588,Japan*

Abstract. We reveal cosmic star-formation history obscured by dust using deep infrared observation with the AKARI. A continuous filter coverage in the mid-IR wavelength (2.4, 3.2, 4.1, 7, 9, 11, 15, 18, and 24μm) by the AKARI satellite allows us to estimate restframe 8μm and 12μm luminosities without using a large extrapolation based on a SED fit, which was the largest uncertainty in previous work. We found that restframe 8μm ($0.38 < z < 2.2$), 12μm ($0.15 < z < 1.16$), and total infrared (TIR) luminosity functions (LFs) ($0.2 < z < 1.6$) constructed from the AKARI NEP deep data, show a continuous and strong evolution toward higher redshift. In terms of cosmic infrared luminosity density (Ω_{IR}), which was obtained by integrating analytic fits to the LFs, we found a good agreement with previous work at $z < 1.2$, with $\Omega_{IR} \propto (1+z)^{4.4\pm1.0}$. When we separate contributions to Ω_{IR} by LIRGs and ULIRGs, we found more IR luminous sources are increasingly more important at higher redshift. We found that the ULIRG (LIRG) contribution increases by a factor of 10 (1.8) from z=0.35 to z=1.4.

Keywords: galaxies: evolution, galaxies:starburst
PACS: 98.70.Lt

***Introduction*.** Revealing the cosmic star formation history is one of the major goals of the observational astronomy. However, UV/optical estimation only provides us with a lower limit of the star formation rate (SFR) due to the obscuration by dust. A straightforward way to overcome this problem is to observe in infrared, which can capture the star formation activity invisible in the UV. The superb sensitivities of recently launched Spitzer and AKARI satellites can revolutionize the field.

However, most of the Spitzer work relied on a large extrapolation from 24μm flux to estimate the 8, 12μm or total infrared (TIR) luminosity, due to the limited number of mid-IR filters. AKARI has continuous filter coverage across the mid-IR wavelengths, thus, allows us to estimate mid-IR luminosity without using a large *k*-correction based on the SED models, eliminating the largest uncertainty in previous work. By taking advantage of this, we present the restframe 8, 12μm TIR LFs, and thereby the cosmic star formation history derived from these using the AKARI NEP-Deep data.

***Data & Analysis*.** The AKARI has observed the NEP deep field (0.4 deg^2) in 9 filters ($N2, N3, N4, S7, S9W, S11, L15, L18W$ and $L24$) to the depths of 14.2, 11.0, 8.0, 48, 58, 71, 117, 121 and 275μJy (5σ)[14]. This region is also observed in $BVRi'z'$ (Subaru), u' (CFHT), FUV, NUV (GALEX), and J, Ks (KPNO2m), with which we computed photo-z with $\frac{\Delta z}{1+z}$=0.043. Objects which are better fit with a QSO template are removed
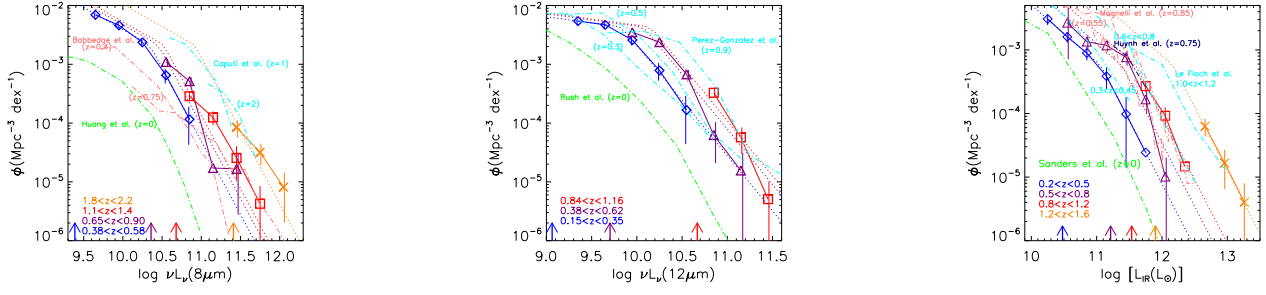
FIGURE 1. (left) Restframe 8μm LFs. The blue diamonds, purple triangles, red squares, and orange crosses show the 8μm LFs at $0.38 < z < 0.58, 0.65 < z < 0.90, 1.1 < z < 1.4$, and $1.8 < z < 2.2$, respectively. The dotted lines show analytical fits with a double-power law. Vertical arrows show the 8μm luminosity corresponding to the flux limit at the central redshift in each redshift bin. Overplotted are Babbedge et al. [1] in the pink dash-dotted lines, Caputi et al. [2] in the cyan dash-dotted lines, and Huang et al. [6] in the green dash-dotted lines. AGNs are excluded from the sample. (middle) Restframe 12μm LFs. The blue diamonds, purple triangles, and red squares show the 12μm LFs at $0.15 < z < 0.35, 0.38 < z < 0.62$, and $0.84 < z < 1.16$, respectively. Overplotted are Pérez-González et al. [11] at z=0.3,0.5 and 0.9 in the cyan dash-dotted lines, and Rush, Malkan, & Spinoglio [12] at z=0 in the green dash-dotted lines. (right) TIR LFs.

from the analysis. We compute LFs using the $1/V_{\max}$ method. Data are used to 5σ with completeness correction. Errors of the LFs are from 1000 realization of Monte Carlo simulation.

8μm LF. Monochromatic 8μm luminosity ($L_{8\mu m}$) is known to correlate well with the TIR luminosity [1, 6], especially for star-forming galaxies because the rest-frame 8μm flux are dominated by prominent PAH features such as at 6.2, 7.7 and 8.6 μm. The left panel of Fig.1 shows a strong evoltuion of 8μm LFs. Overplotted previous work had to rely on SED models to estimate $L_{8\mu m}$ from the Spitzer $S_{24\mu m}$ in the MIR wavelengths where SED modeling is difficult due to the complicated PAH emissions. Here, AKARI's mid-IR bands are advantageous in directly observing redshifted restframe 8μm flux in one of the AKARI's filters, leading to more reliable measurement of 8μm LFs without uncertainty from the SED modeling.

12μm LF. 12μm luminosity ($L_{12\mu m}$) represents mid-IR continuum, and known to correlate closely with TIR luminosity [11]. The middle panel of Fig.1 shows a strong evoltuion of 12μm LFs. Here the agreement with previous work is better because (i) 12μm continuum is easier to be modeled, and (ii) the Spitzer also captures restframe 12μm in $S_{24\mu m}$ at z=1.

TIR LF. Lastly, we show the TIR LFs in the right panel of Fig.1. We used Lagache, Dole, & Puget [8]'s SED templates to fit the photometry using the AKARI bands at $>6\mu$m ($S7, S9W, S11, L15, L18W$ and $L24$). The TIR LFs show a strong evolution compared to local LFs. At $0.25 < z < 1.3$, L_{TIR}^* evolves as $\propto (1+z)^{4.1\pm0.4}$.
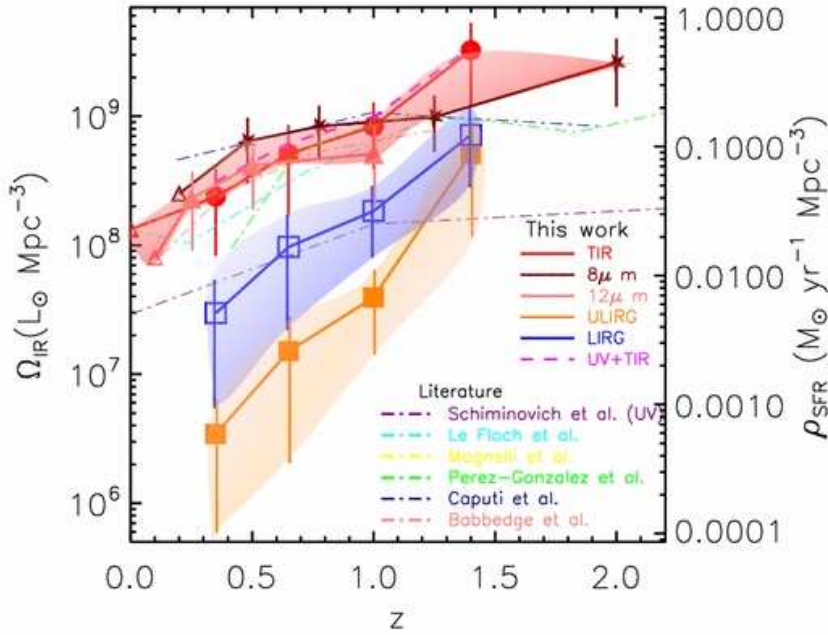
FIGURE 2. Evolution of TIR luminosity density based on TIR LFs (red circles), 8μm LFs (stars), and 12μm LFs (filled triangles). The blue open squares and orange filled squares are for LIRG and ULIRGs only, also based on our L_{TIR} LFs. Overplotted dot-dashed lines are estimates from the literature: Le Floc'h et al. [9], Magnelli et al. [10] , Pérez-González et al. [11], Caputi et al. [2], and Babbedge et al. [1] are in cyan, yellow, green, navy, and pink, respectively. The purple dash-dotted line shows UV estimate by Schiminovich et al. [13]. The pink dashed line shows the total estimate of IR (TIR LF) and UV [13].

Cosmic star formation history.   We fit LFs in Fig.1 with a double-power law, then integrate to estimate total infrared luminosity density at various z. The restframe 8 and 12μm LFs are converted to L_{TIR} using [11, 2] before integration. The resulting evolution of the TIR density is shown in Fig.2. The right axis shows the star formation density assuming Kennicutt [7]. We obtain $\Omega_{IR}(z) \propto (1+z)^{4.4\pm1.0}$. Comparison to Ω_{UV} [13] suggests that Ω_{TIR} explains 70% of Ω_{total} at z=0.25, and that by z=1.3, 90% of the cosmic SFD is explained by the infrared. This implies that Ω_{TIR} provides good approximation of the Ω_{total} at $z > 1$.

In Fig.2, we also show the contributions to Ω_{TIR} from LIRGs and ULIRGs. From z=0.35 to z=1.4, Ω_{IR} by LIRGs increases by a factor of ∼1.6, and Ω_{IR} by ULIRGs increases by a factor of ∼10. More details are in Goto et al. [3].

Spatially-Resolved Spectroscopy of an E+A (post-starburst) System.   We performed a spatially-resolved medium resolution long-slit spectroscopy of a nearby E+A (post-starburst) galaxy system with FOCAS/Subaru [4]. This E+A galaxy has an obvious companion galaxy 14kpc in front (Fig.3, left) with the velocity difference of 61.8 km/s.

We found that Hδ equivalent width (EW) of the E+A galaxy is greater than 7Å galaxy wide (8.5 kpc) with no significant spatial variation. We detected a rotational velocity in the companion galaxy of >175km/s. The progenitor of the companion may have been
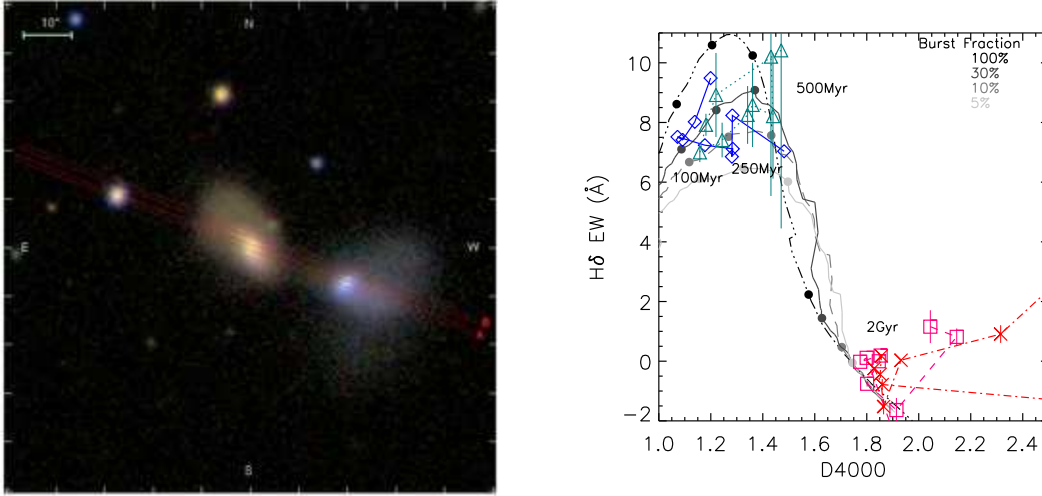
FIGURE 3. (left) The SDSS g,r,i-composite image of the J1613+5103. The long-slit positions are overlayed. The E+A galaxy is to the right (west), with bluer colour. The companion galaxy is to the left (east). (right) Hδ EW is plotted against D4000. The diamonds and triangles are for the E+A core/north spectra, respectively. The squares and crosses are for the companion galaxy's core/north spectra. Gray lines are population synthesis models with 5-100% delta burst population added to the 10G-year-old exponentially-decaying (τ=1Gyr) underlying stellar population. Salpeter IMF and metallicity of $Z = 0.008$ are assumed. On the models, burst ages of 0.1, 0.25, 0.5 and 2 Gyr are marked with the filled circles.

a rotationally-supported, but yet passive S0 galaxy. The age of the E+A galaxy after quenching the star formation is estimated to be 100-500Myr, with its centre having slightly younger stellar population. The companion galaxy is estimated to have older stellar population of >2 Gyrs of age with no significant spatial variation (Fig.3, right).

These findings are inconsistent with a simple picture where the dynamical interaction creates infall of the gas reservoir that causes the central starburst/post-starburst. Instead, our results present an important example where the galaxy-galaxy interaction can trigger a galaxy-wide post-starburst phenomena.

REFERENCES

1. Babbedge T. S. R., et al., 2006, MNRAS, 370, 1159
2. Caputi K. I., et al., 2007, ApJ, 660, 97
3. Goto T., et al. 2010, A&A AKARI special issue
4. Goto T., Yagi M., Yamauchi C., 2008, MNRAS, 391, 700
5. Hopkins A. M., Connolly A. J., Haarsma D. B., Cram L. E., 2001, AJ, 122, 288
6. Huang J.-S., et al., 2007, ApJ, 664, 840
7. Kennicutt R. C., Jr., 1998, ARA&A, 36, 189
8. Lagache G., Dole H., Puget J.-L., 2003, MNRAS, 338, 555
9. Le Floc'h E., et al., 2005, ApJ, 632, 169
10. Magnelli B., et al. 2009, A&A, 496, 57
11. Pérez-González P. G., et al., 2005, ApJ, 630, 82
12. Rush B., Malkan M. A., Spinoglio L., 1993, ApJS, 89, 1
13. Schiminovich D., et al., 2005, ApJ, 619, L47
14. Wada T., et al., 2008, PASJ, 60, 517